J Mater Sci (2012) 47:455–464
DOI 10.1007/s10853-011-5820-1

Effect of TiH_2 particle size distribution on aluminum foaming using the powder metallurgy method

P. M. Proa-Flores · G. Mendoza-Suarez · R. A. L. Drew

Received: 8 April 2011 / Accepted: 25 July 2011 / Published online: 6 August 2011
© Springer Science+Business Media, LLC 2011

Abstract TiH_2 decomposes over a range of temperatures strongly influenced by diverse factors including particle size. In the present research, a systematic study of the dehydrogenation behavior of TiH_2 powder of different particle size distribution was undertaken with the aid of thermogravimetric analysis. The effect of this parameter on aluminum foaming was evaluated. It was found that when TiH_2 exceeds a critical particle size (around 50 μm), dehydrogenation occurs as a single desorption event with onset temperatures around 500 °C. The reduction of particle size, besides reducing the onset of hydrogen release, decreases the dehydrogenation rate. As a result, the first dehydrogenation event gets sharper and tends to overlap with the second with increasing particle size. The use of selected powders on foaming showed that the final foam expansion and porosity features, such as pore size, pore density, and homogeneity are largely influenced by the particle size distribution of the foaming powder. TiH_2 of the largest particle size was the most suitable for foaming pure aluminum.

Abbreviations

PM	Powder metallurgy
FEG-SEM	Field emission electron microscopy
XRD	X-ray diffraction
TG	Thermogravimetric
DTG	Differential thermogravimetric

P. M. Proa-Flores (✉) · G. Mendoza-Suarez
Department of Mining and Materials Engineering, McGill University, Montreal, Canada
e-mail: p_proafl@encs.concordia.ca

P. M. Proa-Flores · R. A. L. Drew
Department of Mechanical & Industrial Engineering, Concordia University, 1459 De Maisonneuve Blvd. West, Montreal, QC H3G 1M8, Canada

Introduction

Aluminum foams are cellular solids that, owing to their closed-cell porous morphology, exhibit an interesting set of physical and mechanical properties[1] with potential application for a wide range of structural components. Among the liquid-processing techniques for aluminum foam processing, the powder metallurgy (PM) method is of particular importance as near-net shapes can be manufactured. However, the technique is still subject of continual effort to optimize the processing variables, improve the foam properties, and reduce the process cost [1, 2]. The PM process takes place in three main steps; the first consists of mixing pure or pre-alloyed aluminum powders with a foaming agent, usually TiH_2. Second, the powder mix is consolidated to obtain a highly dense foam-precursor using techniques like hot pressing or extrusion. Finally, the foam-precursor is heated above the liquidus temperature of the alloy. At this stage, the gas pressure originated from the decomposition reaction of the foaming agent causes the precursor expansion, creating a highly porous semi-solid material that after rapid solidification produces the metallic foam. By foaming inside a mould [3] or by filling hollow profiles [4] further machining can be avoided and light and stiff structural components can be obtained.

[1] Owing to the high degree of porosity that can be achieved, aluminum foams display high stiffness-to-weight ratio, low specific weight, energy absorption during plastic deformation, and good mechanical strength.

To produce good-quality foams, the blowing agent, defined as a material that decomposes under the influence of heat releasing gas, must be non-detrimental to the aluminum alloy. Furthermore, the gas release must proceed as close as possible to the mushy zone of the alloy. The fact that in practice the foaming agent decomposes far before is believed to be one of the causes of a lack of pore uniformity and non-reproducible properties of foams [5]. Up to now, some metallic hydrides, such as TiH_2, ZrH_2, and MgH_2 [6], and carbonates like $MgCO_3$ [7] and $CaCO_3$ [8, 9] have been used in metallic foam's preparation. However, TiH_2 is the most common blowing agent for aluminum foaming as its dehydrogenation reaction is the closest to the melting point of aluminum, and very low contents (around 1 wt%) render a large amount of gas sufficient to create a high degree of porosity. Furthermore, this hydride reversible dehydrogenation reaction is also of interest for hydrogen storage research. TiH_2 decomposition reaction is strongly dependent on several factors, such as particle size [10], amount of initial surface oxidation [11, 12], the atmosphere in which hydrides are heated [6, 11] and heating rate [13]. The hydride dehydrogenation behavior as well as its reaction kinetics have been widely investigated [14–19]. The crystal structure changes of TiH_2 when heated in inert atmospheres are complex. Phase changes are conditioned by the character of phase transformations in the Ti–H system and the processes occurring in the surface layer [20]. The richest phase in hydrogen is γ-TiH_2; at 27 °C, it consists of a f.c.c structure in which lattice positions are occupied by titanium atoms and the tetrahedral interstices are occupied by hydrogen atoms. The range of homogeneity of the γ-phase has been reported to extend over a concentration range of $1.5 < x < 1.94$ (60–66 at.% H) [16]. Within this range, at $TiH_{1.5}$ (60% at.) neutron diffraction has shown that hydrogen atoms are randomly distributed in the tetrahedral interstices of the calcium fluoride type structure [21]. At higher hydrogen concentration ($1.8 < x < 2$), ordered filling of tetrahedral holes occurs, which causes the unit cell to exhibit a tetragonal distortion because of a Jahn–Teller distortion [22]. At lower hydrogen contents ($x \leq 1.5$), β-TiH_2, a b.c.c. phase that may contain up to 50% at. of hydrogen and α-TiH_2 a h.c.p. phase containing minor amounts of hydrogen [20] take place. The dehydrogenation process as observed by differential thermal analyses (in inert atmospheres) is reported to take place in two steps [10, 23]. It has been proposed that the first dehydrogenation event is related to hydrogen losses from γ-TiH_2 within its homogeneity range, caused by the transformations of surface hydride species, and that the second and larger endotherm is associated with the phase transformation process from γ-$TiH_{1.53} \rightarrow \beta$-$TiH_{0.87} + 0.33\ H_2$. Further heating would induce a gradual loss of hydrogen from the β-phase not accompanied by well-defined thermal events [17]. Lavrenko et al. [24], on the other hand, referred to the first endothermic peak as a transfer of hydrogen atoms from tetrahedral to octahedral lattice sites, accompanied by approximately 20% of hydrogen release and related the second endothermic peak to the removal of a larger proportion of the remaining hydrogen from octahedral sites**.** More recently, Bhosle et al. [10] determined that the intermediate phase, TiH_x, is particle size dependent and that x can have values in the range of $0.7 < x < 1.1$. The intermediate phase is formed by the hydride partial dehydrogenation and remains thermally stable at temperatures higher than that of TiH_2 as a consequence of a larger activation energy for decomposition. Furthermore, the onset of dehydrogenation has been found to be particle size dependent. The effect of reducing MgH_2 and TiH_2 particle size on hydrogen release has been explored for the field of hydrogen storage, where low temperatures of decomposition are desirable [10, 25]. In both research studies, an important reduction of the onset temperature of hydrides, decomposition in ultrafine (nanometric) compared to micron-sized powders was observed. For TiH_2, this effect has been attributed to the large surface energy associated with a nanoscale crystal size and to the increase of defect concentration due to the cold work induced by the milling process used for reducing the powder size. Having this precedent in mind, the particle size and thus the surface area of the foaming agent must play an important role in aluminum foaming. This research is motivated by establishing the effect of controlling the TiH_2 particle size in aluminum foam's manufacture, keeping in mind that, during the foaming process, particles of different particle size would release hydrogen at different temperatures, thus having an effect on pore nucleation and foaming efficiency.

Experimental procedure

Pure aluminum powders from Alfa-Aesar were used as the foam matrix. The powders used as foaming agents were: TiH_2 grade G, and TiH_2 grade VM provided by Chemetall GmbH with a specific particle size range, along with TiH_2 powders from Alfa-Aesar with a broader particle size distribution, denominated: TiH_2-AR. Table 1 shows the powder's specifications given by the manufacturer and the powder size spectrum measured using a Laser Scattering Particle Size Distribution Analyzer (Horiba LA-920). The powder oxygen content was determined using a Leco TCH600 simultaneous nitrogen/oxygen/hydrogen analyzer. Alternatively, TiH_2-AR powder was separated into five fractions using a Warman-M4 cyclosizer apparatus. The cyclosizer allows the determination of particle size distribution within the sub-sieve range. It is an elutriator in which a mass of particles is separated into fractions with

Table 1 Properties of the starting materials

Specification by the powder supplier			Measured powder properties				
Powder	Purity (%)	Nominal Size (μm)	D_{10} (μm)	D_{50} (μm)	D_{90} (μm)	Mean diameter (μm)	Oxygen (wt%)
Al	99.5	≤44	8.2	16.6	31.8	18.9	0.39
TiH_2-AR	99	≤44	4.2	14.5	33.4	16.9	0.41
TiH_2-G	min. 98.8	≈60	12.9	49.1	108.2	55.4	0.50
TiH_2-U	min. 98.8	5 ± 1.0 Avg.	4.1	13.4	29.9	16.2	0.55
TiH_2-VM	min. 97.7	1.8 ± 0.2 Avg.	1.9	3.6	5.7	3.7	1.72

the aid of staged hydraulic cyclones, where the particles are separated according to their Stokes equivalent diameter. The effective separating range depends, among other operating factors, on the particle's specific gravity. In this research, for an initial 100 g of TiH_2–AR feed, the cyclosizer was operated at 23 °C, with a water flow of 10.35 L min^{-1} and an elutriation time of 15 min. This way, the effective particle step size was calculated using an overall correction factor of 1.098 [26] that resulted in the nominal particle size ranges reported in Table 2. After separation, the fractions denominated TiH_2-M1, -M2, -M3, -M4, and -M5 were dried at 110 °C for two hours, weighed, and their particle size distribution was measured.

Foaming process

Aluminum foams were prepared following the PM route by mixing the metallic aluminum powder with 1 wt% of selected TiH_2 powder: TiH_2-AR, TiH_2-M4 TiH_2-G and TiH_2-VM. The mixing process was performed in a conventional tumbler mixer for 30 min followed by powder compaction achieved via cold and hot uni-axial pressings. The resulting foamable precursors of 6 g had 98.6 ± 0.2 of theoretical density. The free foaming process was carried out inside a Lindberg/Blue M furnace at 800 °C, and the expansion profile of foams was monitored by interrupted experiments. Constrained foaming to record the volumetric expansion profile of single foams was performed using a laser-expandometer. Details on the equipment construction can be found in Ref. [27]. Using the latter set-up, the temperature profile of precursors was measured by attaching a flexible type K thermocouple into a narrow hole at the bottom of the crucible where foaming took place. In this way a direct contact with the precursor during foaming was assured.

To analyze and characterize the hydride powders, the following characterization techniques were used: Field emission electron microscopy (FEG-SEM) using a Hitachi S-4700; X-ray diffraction (XRD) using a Rigaku Rotaflex Ru-800B with a CuKα_1 ($\lambda = 1.54$ Å) radiation operated at 4.8 kW and thermogravimetric (TG) analysis using a Setaram Evolution-24, which was performed at 10 °C min^{-1} in argon flow. The foam's volumetric expansion was measured using the Archimedes method in at least four samples per foaming time for unconstrained foaming, while for foams manufactured in the laser-expandometer, this measurement was performed in situ. The pore morphology of samples with different expansion degrees was characterized by image analysis. For this evaluation, foams were cross-sectioned parallel to the foam expansion direction, and digital pictures were taken. After increasing the contrast between porosity and foam cell walls, the pore structure characterization was performed using a special routine in Clemex® software. To avoid noise from dark features other than pores, features with areas below 0.25 mm^2 were omitted.

Results and discussion

The inspection of TiH_2 powder via FEG-SEM shows that it possesses an angular morphology. The powder, denominated TiH_2-AR, displays a wide particle size distribution. Using a cyclosizer apparatus, TiH_2-AR was separated into

Table 2 Particle size distribution of TiH_2-AR powder separated by the cyclosizer apparatus

Measured powder properties					
Powder	Nominal size (μm)	D_{10} (μm)	D_{50} (μm)	D_{90} (μm)	Mean diameter
TiH_2-M1	12–16	10.3	14.5	20.7	15.1
TiH_2-M2	16–25	14.4	20.6	27.2	20.8
TiH_2-M3	25–36	20.4	27.6	37.9	28.7
TiH_2-M4	36–48	25.3	35.1	52.3	37.5
TiH_2-M5	≥48	–	–	–	–

five fractions with a particle size step determined using the experimental parameters detailed in the experimental section. Figure 1a–d show micrographs of the original powder and selected fractions. It is observed that the method efficiently separates the powder in fractions of narrow particle size distribution. Except for the fraction M5, in which particle size could not be analyzed because of limited quantity, in the other fractions the particles observed corroborate the data obtained with the particle size analyzer (Table 2). On the other hand, the particle size distribution and micrographs of TiH_2–G show that this powder mean particles size is considerably larger than that of TiH_2-AR, TiH_2-U possesses a similar size distribution, and TiH_2-VM exhibits the smallest mean particle size. For powders obtained from the same source, the powder's oxygen content has a tendency to increase, as the particle size decreases (TiH_2-VM > TiH_2-U > TiH_2-G). Powders of small particle size have a greater affinity for oxygen because of their larger surface area exposed for oxygen adsorption. XRD analysis shows that all the powders have the same stoichiometry and correspond to a $TiH_{1.924}$ phase, containing 3.89 wt% of hydrogen (Fig. 2). Among all, the XRD pattern of TiH_2-VM shows a small degree of peak broadening. The presence of nanosized grains and/or lattice damage might be possible if high-energy milling was used for reducing the powder's particle size. Despite the high oxygen content of some powders (e.g., TiH_2-VM), no oxides peaks were identified.

As stated previously, the hydrogen evolution of TiH_2 is complex, more than one mechanism operates simultaneously, and is manifested as a change of the slope in a TG weight loss curve. This behavior can be clearly observed in the differential thermogravimetric (DTG) pattern, where slope changes are manifested as peaks, and the highest hydrogen desorption rate is found at the minimum of the larger peak of the two dehydrogenation events. Figure 3a, b shows the TG and DTG patterns of as-received powders, respectively. TiH_2-AR shows a hydrogen evolution onset

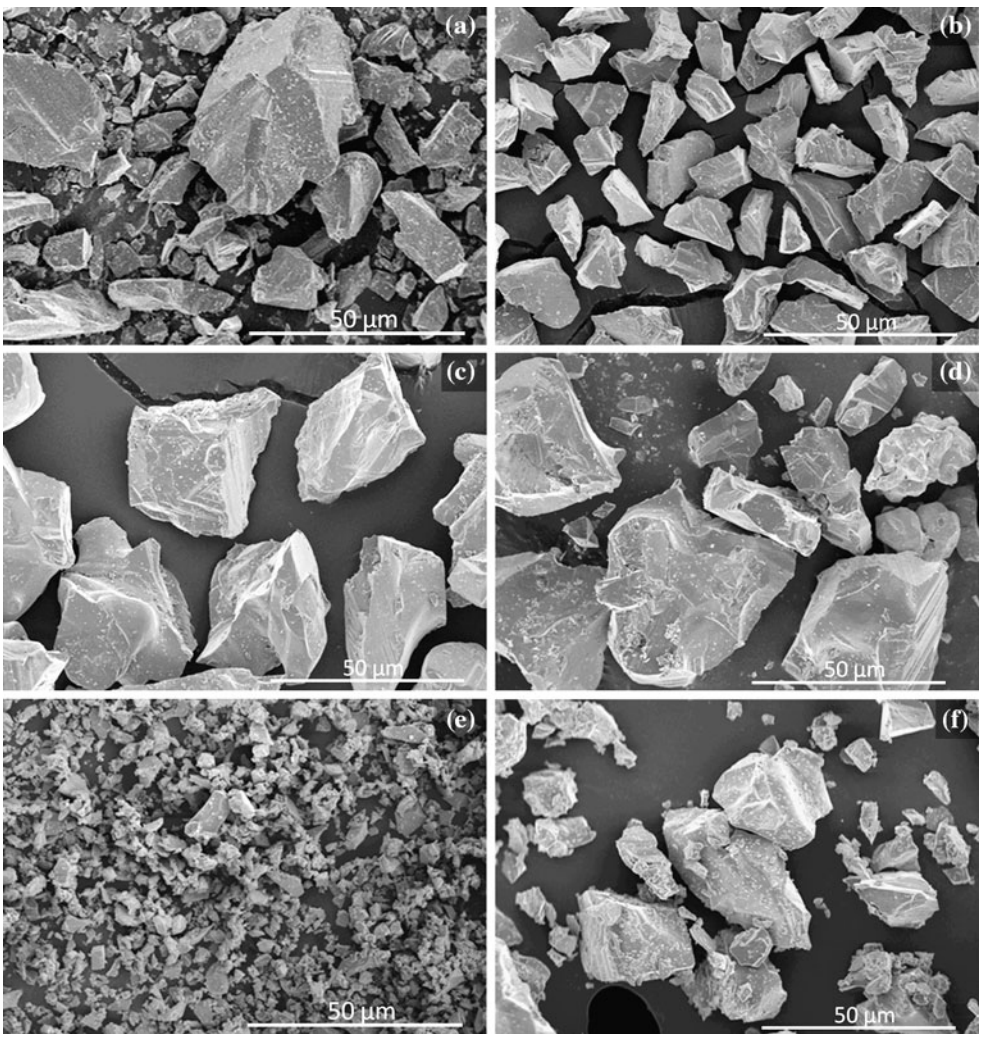

Fig. 1 FEG-SEM images of **a** TiH_2-AR, **b** -M1, **c** -M4, **d** -M5, **e** -VM, and **f** -G powder

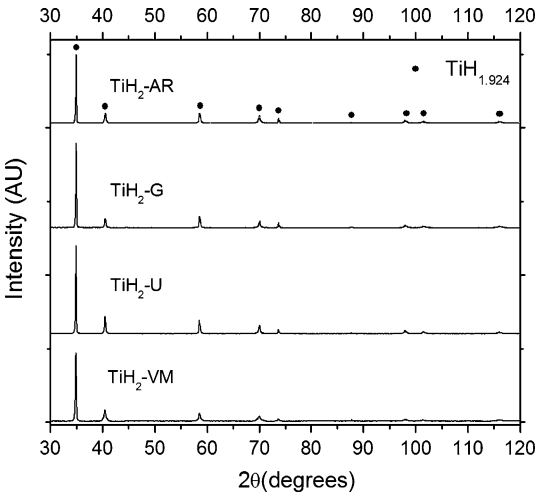

Fig. 2 XRD patterns of TiH_2- AR, -G, -U, and -VM powders. Powder's microstructure corresponds to δ-phase $TiH_{1.924}$

near 460 °C. TiH_2-U, with a similar particle distribution to TiH_2-AR and, disregarding its higher oxygen content, starts to release hydrogen close to 440 °C. TiH_2-G the particle size of which is the largest, also shows the highest dehydrogenation onset around 470 °C. TiH_2-VM, the powder of smaller particle size, releases hydrogen at the lowest temperature (420 °C), even though its high oxygen content implies a thicker surface oxide acting as barrier to hydrogen release. In general, the powder's weight loss is reduced, as their particle size decreases: TiH_2-G loses 3.65 wt%, TiH_2-AR 3.6%, TiH_2-U 3.45 wt%, and TiH_2-VM approximately 2.8 wt%. The TG and DTG patterns of TiH_2-AR fractions (M1 to M5) shown in Fig. 4a, b also demonstrate that the smaller the particle size of fractions the sooner the particles start to release hydrogen. Compared to the bulk, M1 and M2 fractions display slightly lower hydrogen desorption onset temperature; meanwhile, M3, M4 and M5 exhibit a delay of the aforementioned temperature. Furthermore, a consistent reduction in the temperature range of hydrogen release of coarse particles is observed when compared with powders of finer particle size. The end of dehydrogenation of all powder sizes is similar and was determined at the temperature where the DTG traces return to the initial baseline.

The reduction of the onset of dehydrogenation temperature of fine particles has been observed previously and can be attributed to the ease of hydrogen release because of an increased surface area. In addition, if the particle reduction is achieved by milling, then there could be an effect of the rupture of the natural oxide layer that acts as diffusion barrier [10]. In the present research, rather than milling, particles were divided into fractions according to their Stokes settling characteristics, and no plastic deformation was induced; in addition, all powders share the same stoichiometry (Fig. 2). Therefore, the changes observed on the hydrogen evolution onset, especially that of fractions (from TiH_2-M1 to -M5), can be attributed solely to the increase or reduction of powder particle size. For the powders TiH_2-VM, TiH_2-U, and TiH_2-G, on the other hand, a larger effect of the surface oxidation could be expected, since their oxygen content increases as the particle size decreases. Regardless, the smaller particles (TiH_2-VM) release hydrogen sooner than the coarser (TiH_2-U, -G and -AR). The effects of higher oxygen content of small particles are a reduction of their total weight loss and the tendency to gain weight at the end of the TG experiment. As seen, in powder of broad particle size distribution, fine particles determine the onset of dehydrogenation, and by controlling the mean particle size toward coarse particles, the temperature mismatch related to foaming can be reduced.

Furthermore, as observed in the DTG patterns, the relative degrees of dehydrogenation of both peaks change with TiH_2 particle size. For instance, powders like TiH_2-VM and TiH_2-U show two-step dehydrogenation, whereas that of TiH_2-G consists of a peak with an initial shoulder. Similarly, the dehydrogenation behavior of fractions show

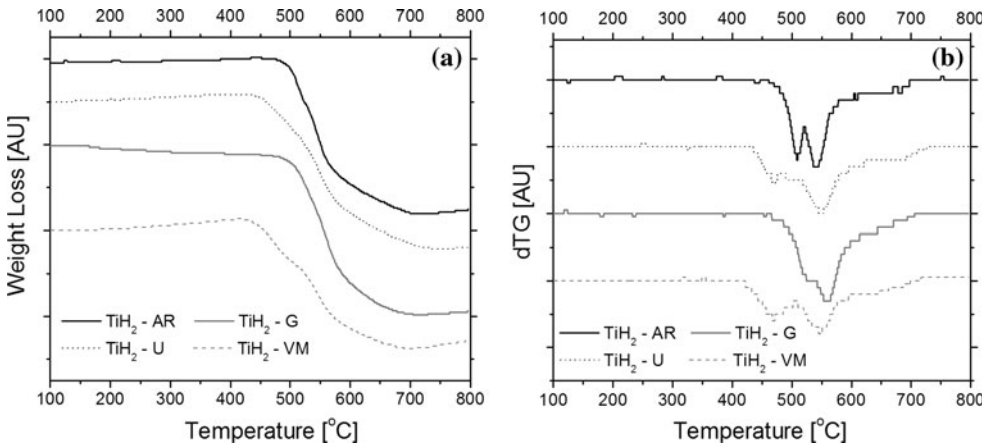

Fig. 3 TG (**a**) and DTG (**b**) patterns of TiH_2- AR, -G, -U, and -VM powders. The experiments were conducted in argon flow at 10°C min^{-1}

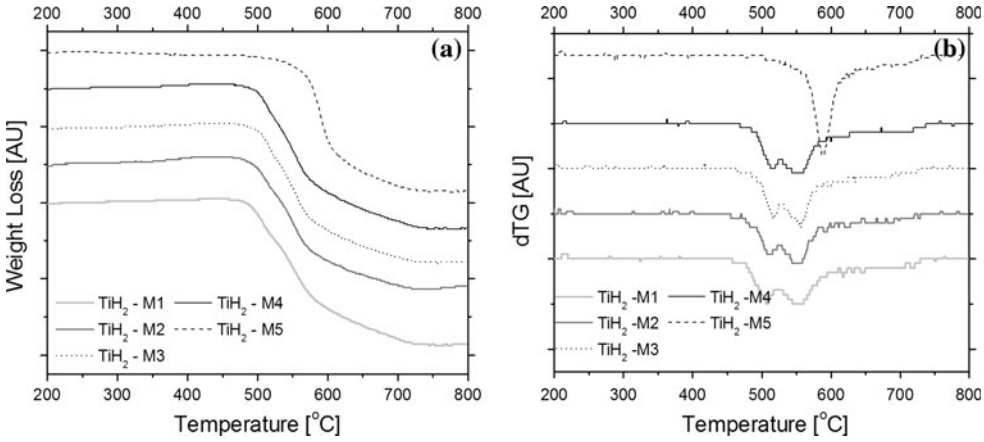

Fig. 4 TG (**a**) and DTG (**b**) patterns of TiH_2-AR fractions. The experiments were conducted in argon flow at 10°C min^{-1}

that when the powder particle size increases, the initial peak seems to shift toward the second, generating a peak overlap and the appearance of a single dehydrogenation event in the coarse TiH_2-M5 powder (characteristic temperatures of DTG patterns are summarized in Table 3). Previously, Bhosle et al. [10] have reported that the intermediate phase TiH_x has a variable range of stability (x was found to vary from $x = 0.7$ to 1.1 for nanometric powders; as the particles size decreases, x tends to lower values), which explains the reduction of weight loss of the initial peak with increasing particle size. In the present research, it is observed that the kinetics of dehydrogenation are also modified by the powder particle size. The first peak related to hydrogen losses from γ-$TiH_{1.924} \rightarrow TiH_x$ becomes noticeably wider for fine powders. If this reaction is delayed to higher temperature but occurs at a faster rate for coarse powder, then the peak overlap seen in TiH_2-G and the appearance of a single peak on TiH_2-M5 can be explained.

The expansion behavior of foams using selected TiH_2 powders is shown in Fig. 5. Most curves illustrate fast foaming followed by rapid decay where a lack of foam stability is evident, resulting from the absence of stabilizing mechanisms in the pure aluminum melt. In both, the constrained and unconstrained foamings, much of the data scatter is localized near the maximum expansion and is larger for foams manufactured with the fine TiH_2-VM powder, and the powder of a wide particle size distribution (TiH_2-AR). Unconstrained foaming shows that when TiH_2-AR is used, a steep expansion slope followed by a small plateau-like region characterizes foaming. Maximum expansions occurring under this condition are around 300%. More reproducible foaming is observed when coarse and narrow-size distribution powders (TiH_2-M4 and TiH_2-G) are used; in both curves, the expansions appear to take place at different stages, and the maximum expansions reached are lower than when using TiH_2-AR. Meanwhile, foams produced with fine TiH_2-VM powder display the poorest foamability as its low onset of dehydrogenation causes a large amount of hydrogen to be lost before the metallic matrix becomes molten, and the maximum volumetric expansion under this condition is less than 200%. The constrained expansion behavior observed by using a laser-expandometer (Fig. 6) is similar to that obtained with interrupted experiments and shows a strong influence of TiH_2 particle size on foaming. In general, the expansion profile can be divided into three stages determined by the temperature of the foam precursor during foaming. Initially, there is a reduced area of contact between the precursor and the mold walls and heat is transferred via conduction; the small increase of volume observed at this stage corresponds to precursor dilation. Once the temperature reached is near the melting point of aluminum, the precursor softens, increasing its volume three dimensionally, until it assumes

Table 3 Onset of dehydrogenation and peak temperatures of the foaming agent powder

Powder	Temperature (°C)			Powder	Temperature (°C)		
	Onset	Peak I	Peak II		Onset	Peak I	Peak II
TiH_2-AR	460	508	540	TiH_2-M1	457	508	550
TiH_2-VM	420	467	545	TiH_2-M2	457	510	550
TiH_2-U	440	470	547	TiH_2-M3	470	520	557
TiH_2-G	469	–	552	TiH_2-M4	470	520	557
				TiH_2-M5	500	–	585

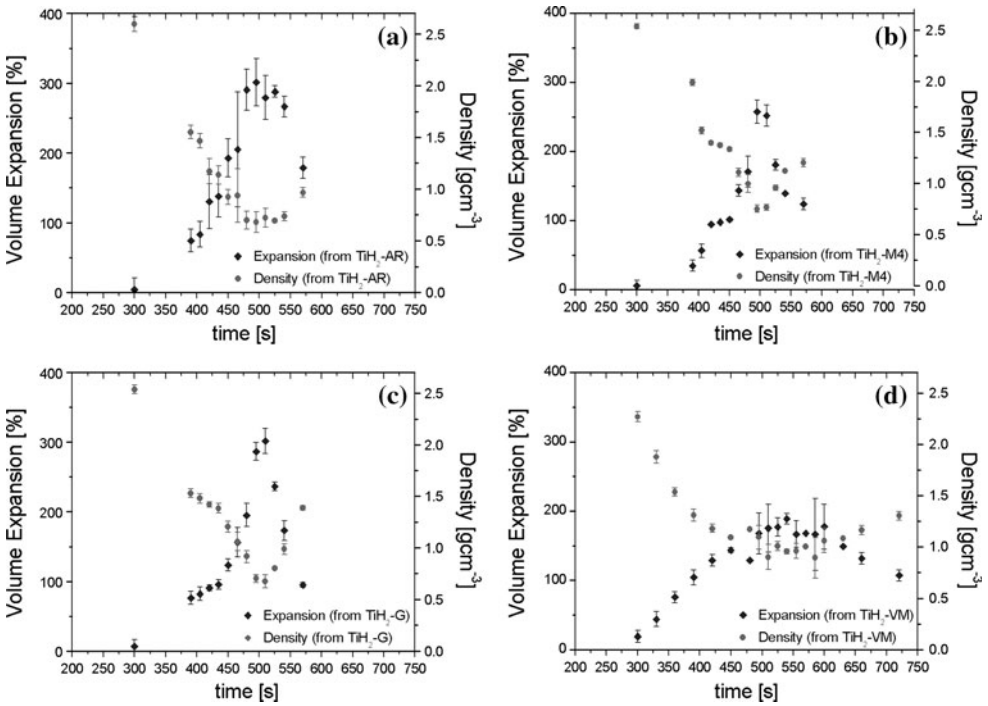

Fig. 5 Expansion and density profiles of foams produced with **a** TiH_2-AR, **b** TiH_2-M4, **c** TiH_2-G, and **d** TiH_2-VM powders

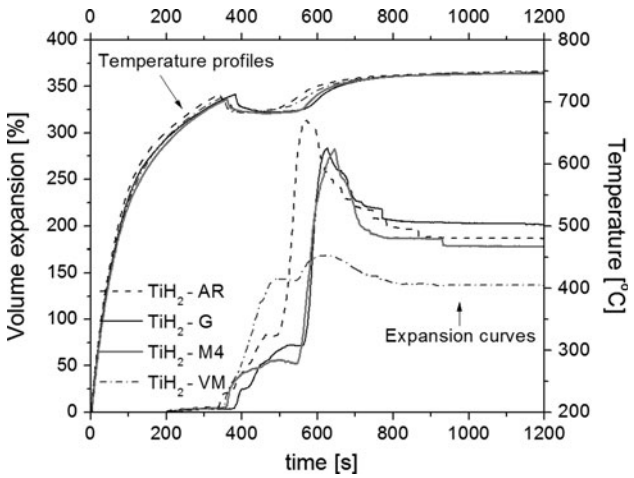

Fig. 6 Expansion and precursor temperatures profiles obtained using the laser-expandometer

the contour of the mold, and this is observed as a second stage of foaming characterized by a slow expansion at a nearly constant temperature. During the third stage, as a result of the increased transfer of heat, the precursor temperature increases while its viscosity reduces, and rapid foaming takes place. Because there is no mechanism preventing the flow of liquid in the cell walls, drainage and foam decay proceed rapidly together with a temperature increase. Similarly, the higher expansions reached are found with the wide particle size distribution of TiH_2-AR, followed by the large particle sizes of TiH_2-G and TiH_2-M4 powders. Fine powder (TiH_2-VM) is not efficient for aluminum foaming as their dehydrogenation temperature is very low such that much of the hydrogen gas is lost in the initial stage of foaming, generating reduced expansions.

The foam development observed in Fig. 7 shows that the powder's particle size strongly affects the way porosity nucleates and distributes at early stages of foaming. Initially, crack-like pores tend to become rounder as the metal softens, and the surface tension effect of the liquid aluminum grows in importance. With time, pore density decreases, whereas the mean pore diameter grows; finally, when the cell walls stretch beyond a critical value, bubble bursting takes place, and foam collapse starts. The rupture of the thin films is mainly produced by the drainage phenomena observed in all the foams after the maximum expansion levels are reached. Foams produced with TiH_2-AR display an heterogeneous pore morphology and a broad pore size distribution. After 510 s, the foams still conserve their lowest density; however, the pore structure consists of large coalesced pores. The intensive pore coalescence observed is the reason for the highly non-reproducible foaming process observed in Fig. 4. The porosity features observed using TiH_2-M4, on the other hand, exhibit homogeneous and uniformly distributed pores. Initially, the compacts expand with a similar rate as that of TiH_2-AR, but as pores develop, the expansion rate decreases. At maximum expansion, the foam morphology is characterized by rounded homogeneous pores; nevertheless, foam collapse in this case occurs sooner than when TiH_2-AR is used. The fact that the onset of hydrogen evolution of TiH_2-M4 powder is 10 °C higher than that of TiH_2-AR

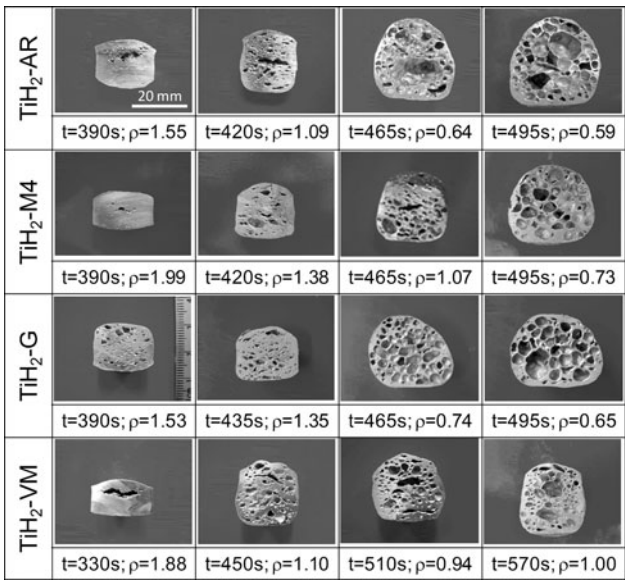

Fig. 7 Evolution of pore morphology for foams manufactured with TiH_2-AR, TiH_2-M4, TiH_2-G and TiH_2-VM. Densities (ρ) are reported in g cm^{-3}

does not impact the initial foam expansion; however, differences in foam morphology are clearly visible. The pore development for TiH_2-G is similar; pores nucleate more homogeneously and are distributed in the aluminum matrix. Even though the expansions reached are lower than those of the foams manufactured using TiH_2-AR, these foams display better porosity features (homogenous pores of narrow size distribution). Nonetheless, the time frame to freeze the foam after reaching the maximum expansion is short. Finally, the pore morphology of foams manufactured with TiH_2-VM consists mostly of oblate pores. The premature gas release in the precursor causes the formation of macroscopic cracks, and as a result, large amounts of gas escape from the foamable precursor, and foam expansion is reduced. Pores tend to become rounder at the maximum expansion (around 510 s), but the quantity of coalesced pores is significant.

Figure 8 shows the pore area distribution of aluminum foams at maximum expansion. Foams produced with TiH_2-AR and -VM show outlier values at the 24–32 mm^2 interval, indicative of the large pores found under these conditions. The narrowest pore area distribution is obtained when foaming with TiH_2-G, and the broader distribution is found when TiH_2-AR is used, followed by the use of TiH_2-VM. Foams produced with TiH_2-M4 fall in between, displaying a narrower distribution than foams produced with TiH_2-AR, but larger than those produced with TiH_2-G. The smaller porosity was found with TiH_2-VM, where roughly 87% of the pores counted have an area below 4 mm^2, while for all other conditions, the amount of pores below this number is around 73% (Fig. 8b).

The porosity aspect ratio, defined as the ratio between the pore length perpendicular and the pore length in the expansion direction, is presented in Fig. 9. For all the foams tested, the majority of pores are elongated perpendicular to the direction of foam expansion (values >1). The largest number of oblate pores is found for TiH_2-VM, followed by TiH_2-AR foams. On the other hand, foams produced with TiH_2-G and -M4 present the smallest number of pores of high aspect ratios, indicative of a more regular pore structure.

The average values of pore density, area of pores calculated from image analysis, and the relative densities calculated with the bulk of foams are summarized in Table 4. In general, the pore density increases, and the foam area occupied by pores decreases as the particle size of TiH_2 decreases. The highest relative density is exhibited for foams produced with the finer TiH_2-VM powder, while the lightest foams are found when using TiH_2-AR powder.

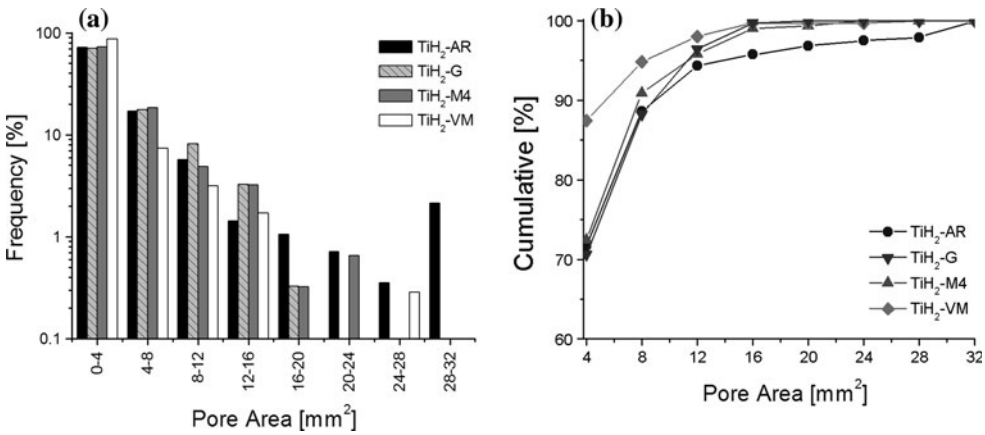

Fig. 8 **a** Frequency and **b** cumulative charts of the pore area distributions of foams produced from TiH_2 of different particle sizes

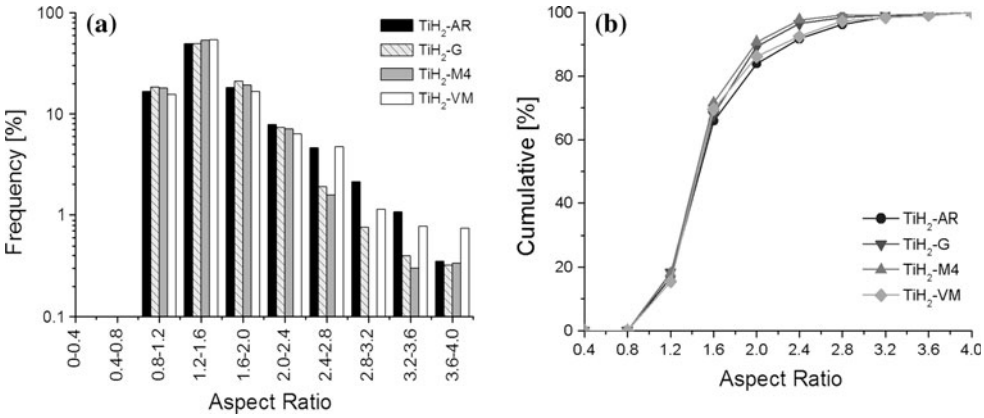

Fig. 9 **a** Frequency and **b** cumulative charts of the pore aspect ratios of aluminum foams produced from TiH_2 of different particle size

Table 4 Pore density, pore area, and relative density of foams manufactured with different TiH_2 powders

Foaming agent	Pore density (n)	Std. dev.	Pore area (%)	Std. dev.	Rel. density (ρ^*/ρ)	Std. dev.
TiH_2-AR	71	9	63.7	4.8	0.22	0.01
TiH_2-AR M4	77	8	55.2	3.6	0.32	0.04
TiH_2-G	66	9	62.0	4.6	0.27	0.03
TiH_2-VM	93	15	50.5	5.4	0.35	0.03

Conclusions

The thermal decomposition of titanium hydride powders is a complex process strongly modified by the powder particle size. The dehydrogenation process occurs at higher temperature and at faster rate with the increase of particle size, generating a single desorption peak in TiH_2 when the powder particle size is around 50 μm (TiH_2-M5). By controlling the hydride's particle size, the hydrogen evolution onset can be modified to temperatures closer to the liquidus temperature of the aluminum alloy. Coarse titanium hydride powders of D_{50} = 49.1 μm (TiH_2-G) display a hydrogen evolution onset nearly 50 °C above that of fine powders of D_{50} = 3.6 μm (TiH_2-VM). For the PM processing route the use of TiH_2 of controlled particle size influences foam expansion and porosity features, such as pore size, pore density, and homogeneity. Coarse TiH_2 powder was found to be more suitable to foam aluminum powder.

Acknowledgments The authors would like to thank the following organizations for partial funding in the present research: General Motors Canada; The Natural Sciences and Engineering Research Council of Canada (NSERC); and The Fonds Québécois de la Recherche sur la Nature et les Technologies (FQRNT); The authors would also like to thank the Consejo Nacional de Ciencia y Tecnología (CONACyT) México, for providing a scholarship to Paula M. Proa-Flores.

References

1. Nosko M, Simancik F, Florek R (2010) Mat Sci Eng A 527 (21–22):5900
2. Hohlfeld J, Hannemann C, Vogel R, Hipke T, Neugebauer R (2011) Prod Eng Res Dev 5(1):25
3. Stobener K, Rausch G (2009) J Mater Sci 44(6):1506. doi: 10.1007/s10853-008-2786-8
4. Bonaccorsi L, Proverbio E, Raffaele N (2010) J Mater Sci 45(6):1514. doi:10.1007/s10853-009-4115-2
5. Lehmhus D, Busse M (2004) Adv Eng Mater 6(6):391
6. Zeppelin FV, Hirscher M, Stanzick H, Banhart J (2003) Compos Sci Technol 63(16):2293
7. Park C, Nutt SR (2000) Mater Sci Eng A 288(1):111
8. Gergely V, Curran DC, Clyne TW (2003) Compos Sci Technol 63(16):2301
9. Cambronero LEG, Ruiz-Roman JM, Corpas FA, Prieto JMR (2009) J Mater Process Technol 209(4):1803
10. Bhosle V, Baburaj EG, Miranova M, Salama K (2003) Mater Sci Eng A 356(1–2):190
11. Lehmhus D, Rausch G (2004) Adv Eng Mater 6(5):313
12. Matijasevic-Lux B, Banhart J, Fiechter S, Görke O, Wanderka N (2006) Acta Mater 54(7):1887
13. Kennedy AR (2002) Scripta Mater 47(11):763
14. Zschommler-Sandim HR, Vieira-Morante B, Atsushi-Suzuki P (2005) Mater Res 8(3):293
15. Matysina ZA, Shchur DV (2001) Russ Phys J 44(11):1237
16. San-Martin A, Manchester FD (1987) J Phase Equilib 1:30
17. Padurets LN, Shilov AL (1997) Zh Neorg Khim 42(8):1258
18. Padurets LN, Dobrokhotova ZV, Shilov AL (1999) Int J Hydrogen Energy 24(2–3):153
19. Fokin VN, Malov YI, Fokina EE, Troitskaya SL, Shilkin SP (1995) Int J Hydrogen Energy 20(5):387

20. Kobzenko GF, Kobzenko AP, Chubenko MV, Pet'kov VV, Polenur AV (1995) Int J Hydrogen Energy 20(5):383
21. Bale HD, Peterson BS (1972) Solid State Comm 11(9):1143
22. Fujimori A, Tsuda N (1982) J Less Common Met 88(2):269
23. Matijasevic B, Fiechter S, Zizak I (2004) In: Danninger H, Ratzi R (eds) Powder metallurgy world congress, Vienna, 2004. European Powder Metallurgy Association, Shrewsbury, pp 149–155
24. Lavrenko VA, Shemet VZ, Petrov LA, Teplov OA, Dolukhanyan SK (1990) Oxid Met 33(1–2):177
25. Varin RA, Czujko T, Wronski Z (2006) Nanotechnology 17(15):3856
26. Anon (1997) Particle Size Analysis in the sub-sieve range. Cyclosizer Instruction Manual, Bulletin WCS/2, 3rd edn, Artamon Australia
27. Proa-Flores PM (2010) Aluminium foams fabricated by the pm route using nickel-coated titanium hydride powders of controlled particle size. McGill University, Montreal